Chapter 1.

Chiral texture in toroidal liquid crystals

Nematic liquid crystals can be thought of as liquids compounds of elongated particles which tend to be axially aligned. The elongated particles can be thought of as rod-like molecules with a typical size of few nanometers. The nematic order refers to the alignment in the orientation of the rods, which is the ground state of nematic liquid crystals. Mathematically, nematic liquid crystals can be described by a double headed vector field $\mathbf{n}(\mathbf{x})$, often called the director field. The director field is assumed to align with the average orientation of the particles in a small patch. As the particles — or rods — are biaxially symmetric, their orientation is locally invariant under a rotation of π radians. Hence, an energy $F[\mathbf{n}(\mathbf{x})]$ describing such particles should be invariant under the following transformation:

$$F[\mathbf{n}(\mathbf{x})] = F[-\mathbf{n}(\mathbf{x})]. \tag{1.1}$$

As the director field purely contains orientational information we will assume $\mathbf{n}(\mathbf{x})^2 = 1$ for any given $\mathbf{x}$; the directory field is a unitary vector field.

As nematic liquid crystals align to yield the lowest-energy configuration, any distortion from this alignment comes at an energetic cost [119, 132, 154]. To account for these energetic costs, a phenomenological energy is constructed, called the Frank free energy $F[\mathbf{n}(\mathbf{x})]$. As the Frank free energy is essentially an elastic energy, for a strain u_{ij} the most general form is given by

$$F = \tfrac{1}{2} \int \mathrm{d}V \, K_{ijkl} u_{ij} u_{kl}, \tag{1.2}$$

where K_{ijkl} is the elastic tensor. In the case of a nematic, the strain is given by the gradient of the nematic director field $u_{ij} = \nabla_i n_j$, which yields

$$F = \tfrac{1}{2} \int \mathrm{d}V \, K_{ijkl} \nabla_i n_j \nabla_k n_l. \tag{1.3}$$

In three dimensions, the elastic tensor K_{ijkl} has only three independent components in the bulk due to the biaxial properties of the energy and the unitariness of $\mathbf{n}(\mathbf{x})$. This results in three terms. The first term, the splay energy, is given by

$$F_1 = \tfrac{1}{2} \int \mathrm{d}V \, K_1 (\nabla \cdot \mathbf{n})^2. \tag{1.4}$$

The second term, the twist energy is given by

$$F_2 = \tfrac{1}{2} \int \mathrm{d}V \, K_2 (\mathbf{n} \cdot \nabla \times \mathbf{n})^2. \tag{1.5}$$

The third term, the bend energy is given by

$$F_3 = \tfrac{1}{2} \int \mathrm{d}V \, K_3 (\mathbf{n} \times \nabla \times \mathbf{n})^2. \tag{1.6}$$

It turns out, however, that there is also a physically relevant surface term: saddle-splay, given by: [119]

$$F_{24} = -K_{24} \int \mathbf{dS} \cdot \left(\mathbf{n} \nabla \cdot \mathbf{n} + \mathbf{n} \times \nabla \times \mathbf{n} \right). \tag{1.7}$$

The total Frank free energy for nematic liquid crystals confined in a space is the sum of all these energies, as given by eq. (1.8).

At low temperatures, the nematic liquid crystal would like to align completely throughout space, as it yields the lowest-energy state. This is, however, not always possible due to the geometry and topology of the confining space.

1.1 Toroidal confinements

The confinement of liquid crystals in non-trivial geometries forms a rich and interesting area of study because the preferred alignment at the *curved* bounding surface induces bulk distortions of the liquid crystal — that is, the boundary conditions *matter*. This results in a great diversity of assemblies and

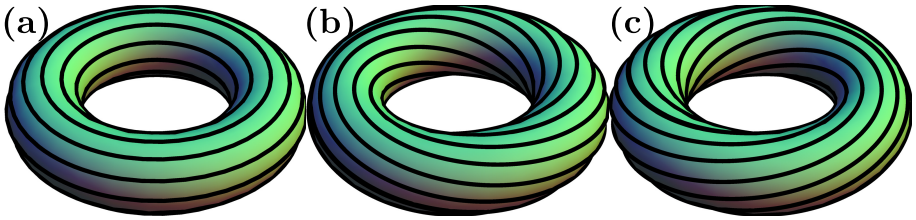

Figure 1.1: Schematic of (a) achiral, (b) right-handed and (c) left-handed toroidal nematic liquid crystals. The black lines are director field lines on the bounding torus.

mechanical phenomena [72, 130, 137, 138, 146]. Water droplets dispersed in a nematic liquid crystal interact and assemble into chains due to the presence of the anisotropic host fluid [139, 141, 145], defect lines in cholesteric liquid crystals can be knotted and linked around colloidal particles [71, 77, 100, 101], and surface defects in spherical nematic shells can abruptly migrate when the thickness inhomogeneity of the shell is altered [50, 73]. In these examples, spherical droplets (or colloids), either filled with — or dispersed in — a liquid crystal, create architectures arising from their coupling to the orientational order of the liquid crystal. Nematic structures where the bounding surface of the colloid or the liquid crystal droplet is topologically different from a sphere have also been studied [45, 51, 60]. Though there has been much interest in the interplay between order and toroidal geometries [45, 63, 74, 90, 96, 97, 112, 114, 135], it was only recently that experimental realisations of nematic liquid crystal droplets with toroidal boundaries were reported [55, 86]. Polarised microscopy revealed a twisted nematic orientation in droplets with planar degenerate (tangential) boundary conditions, despite the achiral nature of nematics. This phenomenon, which we will identify as spontaneous chiral symmetry breaking♠, is subject of theoretical study in this article. The chirality of nematic toroids is displayed by the local average orientation of the nematic molecules, called the director field and indicated by the unit vector $\mathbf{n}$. Motivated by experiment, we will assume this director field to be aligned in the tangent plane of the bounding torus. Figure 1.1a shows an achiral nematic toroid which has its fieldlines aligned along the azimuthal direction, $\hat{\phi}$. In contrast, the chiral nematic toroids in fig. 1.1 b and fig. 1.1 c show a right- and left-handedness, respectively, when following the fieldlines anticlockwise (in the azimuthal direction).

♠Technically, it is spontaneous *achiral* symmetry breaking since the symmetry is the *lack* of chirality. We will, however, conform to the standard convention.

The origin of the chirality lies in two elastic effects of geometric confinement. Firstly, there is a trade-off between bend and twist deformations. Secondly, another type of director distortion called saddle-splay couples the director to the curvature of the boundary, and can consequently favor the chiral state.

These nematic toroids share similarities with polymer bundles [53, 75, 83, 92, 93, 114, 143]. In fact, twisted DNA toroids have been analysed with liquid crystal theory [68, 75, 114]. Under the appropriate solvent conditions DNA condenses into toroids [143, 166]. These efficient packings of genetic material are interesting as vehicles in therapeutic gene delivery; it has been argued [114] that a twist in DNA toroids, for which there are indications both in simulations [122, 131] and experiments [118], would unfold more slowly and could therefore be beneficial for this delivery process. Thus, besides a way to engineer complex structures, the theory of geometrically confined liquid crystals may also provide understanding of biological systems.

The organisation of this article is as follows. In section 1.2 we will discuss our analytical method, which involves a single variational ansatz only for the director fields of both chiral and achiral toroidal nematics. In section 1.3 we will consider its energetics in relation to the slenderness, elastic anisotropies, cholesteric pitch and external fields, and discuss the achiral–chiral transition in the light of the mean field treatment of the Ising model.

1.2 Toroidal director fields

1.2.1 Free energy of a nematic toroid

We will study the general case in which the director lies in the tangent plane of the boundary assuming that the anchoring is strong so that the only energy arises from elastic deformations captured by the Frank free energy functional [119, 154]:

$$\begin{aligned} F[\mathbf{n}(\mathbf{x})] = \frac{1}{2}\int \mathrm{d}V \Big(& K_1(\nabla\cdot\mathbf{n})^2 \\ & + K_2(\mathbf{n}\cdot\nabla\times\mathbf{n})^2 + K_3(\mathbf{n}\times\nabla\times\mathbf{n})^2\Big) \\ & - K_{24}\int \mathbf{dS}\cdot(\mathbf{n}\nabla\cdot\mathbf{n}+\mathbf{n}\times\nabla\times\mathbf{n}), \end{aligned} \tag{1.8}$$

where $\mathrm{d}\mathbf{S} = \boldsymbol{\nu}\,\mathrm{d}S$ is the area element, with $\boldsymbol{\nu}$ the unit normal vector (outward pointing) and where $\mathrm{d}V$ is the volume element. Due to the anisotropic nature of the nematic liquid crystal, this expression contains three bulk elastic moduli, K_1, K_2, K_3, rather than a single one for fully rotationally symmetric systems. In addition, there is a surface elastic constant K_{24}. K_1, K_2, K_3 and K_{24} measure the magnitude of splay, twist, bend and saddle-splay distortions, respectively. We now provide a geometrical interpretation of the saddle-splay distortions. Firstly, observe that under perfect planar anchoring conditions $\mathbf{n} \cdot \boldsymbol{\nu} = 0$, so the first term in the saddle-splay energy does not contribute:

$$F_{24} = -K_{24} \int \mathrm{d}S\; \boldsymbol{\nu} \cdot (\mathbf{n} \times \nabla \times \mathbf{n})\,. \tag{1.9}$$

This remaining term in the saddle-splay energy is often rewritten as

$$F_{24} = K_{24} \int \mathrm{d}S\; \boldsymbol{\nu} \cdot (\mathbf{n} \cdot \nabla)\,\mathbf{n}, \tag{1.10}$$

because

$$\begin{aligned} (\mathbf{n} \times \nabla \times \mathbf{n})_a &= \epsilon_{abc} n_b \epsilon_{cpq} \partial_p n_q \\ &= (\delta_{ap}\delta_{bq} - \delta_{aq}\delta_{bp})\, n_b \partial_p n_q \\ &= -n_b \partial_b n_a \end{aligned} \tag{1.11}$$

where in the last line the identity $0 = \partial_a (1) = \partial_a (n_b n_b) = 2 n_b \partial_a n_b$ is used. In other words, the bend is precisely the curvature of the integral curves of $\mathbf{n}$. Employing the product rule of differentiation $0 = \partial_a (\nu_b n_b) = \nu_b \partial_a n_b + n_b \partial_a \nu_b$ yields:

$$F_{24} = -K_{24} \int \mathrm{d}S\; \mathbf{n} \cdot (\mathbf{n} \cdot \nabla)\,\boldsymbol{\nu}. \tag{1.12}$$

Upon writing $\mathbf{n} = n_1 \boldsymbol{e}_1 + n_2 \boldsymbol{e}_2$, with $\boldsymbol{e}_1$ and $\boldsymbol{e}_1$ two orthonormal basis vectors in the plane of the surface, one obtains

$$F_{24} = K_{24} \int \mathrm{d}S\; n_i L_{ij} n_j, \tag{1.13}$$

where we note that $i, j = 1, 2$ (rather than running till 3). Thus the nematic director couples to the extrinsic curvature tensor [126], defined as

$$L_{ij} = -\boldsymbol{e}_i \cdot (\boldsymbol{e}_j \cdot \nabla)\,\boldsymbol{\nu}. \tag{1.14}$$

If $\boldsymbol{e}_1$ and $\boldsymbol{e}_2$ are in the directions of principal curvatures, κ_1 and κ_2, respectively, one finds:

$$F_{24} = K_{24} \int dS \left(\kappa_1 n_1^2 + \kappa_2 n_2^2\right). \tag{1.15}$$

We conclude that the saddle-splay term favors alignment of the director along the direction with the smallest principal curvature if $K_{24} > 0$. The controversial surface energy density $K_{13}\mathbf{n}\nabla \cdot \mathbf{n}$ is sometimes incorporated in eq. (1.8), but is in our case irrelevant, because the normal vector is perpendicular to $\mathbf{n}$, and so $\mathbf{n} \cdot \boldsymbol{\nu} = 0$.

We will consider a nematic liquid crystal confined in a handle body bounded by a torus given by the following implicit equation for the Cartesian coordinates x, y, and z:

$$\left(R_1 - \sqrt{x^2 + y^2}\right)^2 + z^2 \leq R_2^2. \tag{1.16}$$

Here, R_1 and R_2 are the large and small radii, respectively, of the circles that characterise the outer surface: a torus obtained by revolving a circle of radius R_2 around the z-axis (fig. 1.2).

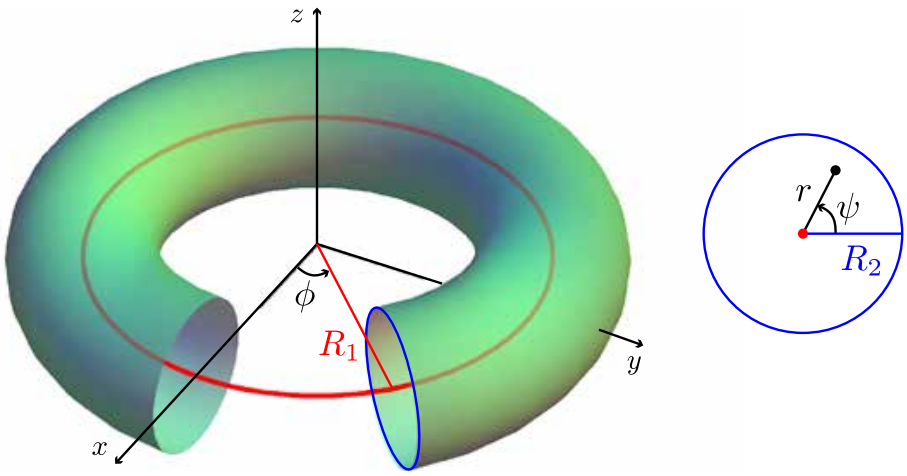

Figure 1.2: *Left panel*: Schematic of the boundary of the geometry-specified eq. (1.16) including graphical definitions of ϕ and R_1. The torus is characterised by a large (red) and a small (blue) circle. The large circle, or centerline, has radius R_1. *Right panel*: Schematic of a cut including graphical definitions of r, ψ and R_2.

We can conveniently parametrise this solid torus by the coordinates $r \in [0, R_2]$, $\phi \in [0, 2\pi)$ and $\psi \in [0, 2\pi)$ (illustrated in fig. 1.2):

$$x = (R_1 + r\cos\psi)\cos\phi, \tag{1.17}$$

$$y = (R_1 + r\cos\psi)\sin\phi, \tag{1.18}$$

$$z = r\sin\psi. \tag{1.19}$$

The metric reads:

$$g_{\mu\nu} = \begin{pmatrix} 1 & 0 & 0 \\ 0 & (R_1 + r\cos\psi)^2 & 0 \\ 0 & 0 & r^2 \end{pmatrix}, \tag{1.20}$$

with $\mu, \nu \in \{r, \phi, \psi\}$. It follows that $\mathrm{d}\mathbf{S} = \boldsymbol{\nu}\sqrt{g}\ \mathrm{d}\psi\,\mathrm{d}\phi$ and $\mathrm{d}V = \sqrt{g}\ \mathrm{d}r\,\mathrm{d}\psi\,\mathrm{d}\phi$, where $g = \det g_{\mu\nu}$.

For a torus the ϕ and ψ directions are the principal directions. The curvature along the ψ direction is negative everywhere (measured with respect to the outward pointing normal) and the smallest of the two, so when $K_{24} > 0$, the director tends to wind along the small circle with radius R_2.

1.2.2 Double twist

To minimise the Frank energy we formulate a variational ansatz built on several simplifying assumptions [114]. We consider a director field which has no radial component (i.e. $n_r = 0$), is tangential to the centerline ($r = 0$), and is independent of ϕ. Furthermore, since we expect the splay (K_1) distortions to be unimportant, we first take the field to be divergence-free (i.e. $\nabla \cdot \mathbf{n} = 0$). Recalling that in curvilinear coordinates the divergence is $\nabla \cdot \mathbf{n} = \frac{1}{\sqrt{g}}\partial_\mu\left(\sqrt{g}n^\mu\right)$, we write

$$n_\psi = \frac{f(r)\,R_1}{\sqrt{g_{\phi\phi}}}, \tag{1.21}$$

where the other terms in $\sqrt{g}$ play no role as they are independent of ψ. The ϕ-component of the director follows from the normalisation condition. For the radial dependence of $f(r)$ we make the simplest choice,

$$f(r) = \frac{\omega r}{R_2}, \tag{1.22}$$

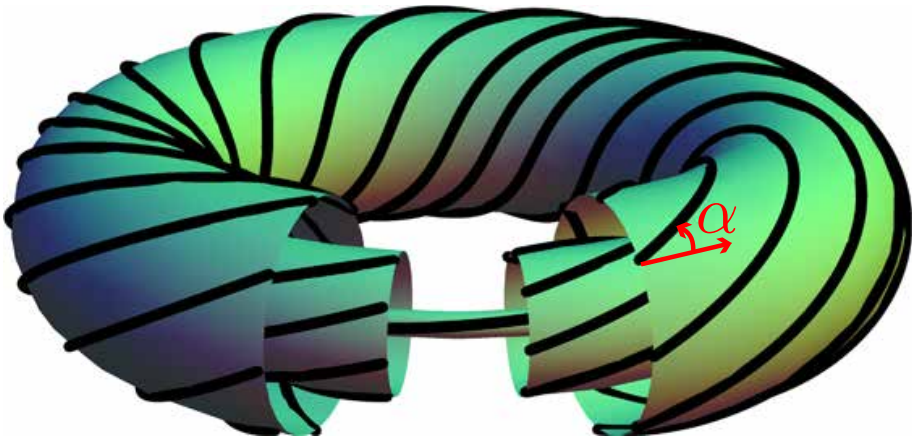

Figure 1.3: Schematic of the ansatz for the director fieldlines ($\omega = 0.6$ and $\xi = 3$), displaying a twist when going radially outward, including a graphical definition of α.

and obtain

$$n_\psi = \omega \frac{\xi r/R_2}{\xi + \frac{r}{R_2}\cos\psi}, \tag{1.23}$$

where we have introduced $\xi \equiv R_1/R_2$, the slenderness or aspect ratio of the torus. The variational parameter ω governs the chirality of the toroidal director field. If $\omega = 0$ the director field corresponds to the axial configuration in fig. 1.1 a. The sign of ω determines the chirality: right-handed when $\omega > 0$ (fig. 1.1 c) and left-handed when $\omega < 0$ (fig. 1.1 b). The magnitude of ω determines the degree of twist. Note that the direction of twist is in the radial direction, as illustrated in fig. 1.3. Therefore the toroidal nematic is doubly twisted, resembling the cylindrical building blocks of the blue phases [119, 154]. It may be useful to relate ω to a quantity at the surface, say the angle, α, that the director makes with $\hat{\phi}$. For the ansatz, this angle will be different depending on whether one measures at the inner or outer part of the torus, but for large ξ we find:

$$\omega \approx n_\psi \left(r = R_2\right) = \sin\alpha. \tag{1.24}$$

1.3 Chiral symmetry breaking

1.3.1 Results for divergence-free field

Since ω only determines the chirality of the double-twisted configuration but not the amount of twist, the free energy is invariant under reversal of the sign of ω, i.e. $F(-\omega) = F(\omega)$. This mirror symmetry allows us to write down a Landau-like expansion in which F only contains even powers of ω,

$$F = a_0(\{K_i\}, \xi) + a_2(\{K_i\}, \xi)\,\omega^2 + a_4(\{K_i\}, \xi)\,\omega^4 + \mathcal{O}\left(\omega^6\right) \tag{1.25}$$

where $\{K_i\}$ is the set of elastic constants.[♠] If the coefficient $a_2 > 0$, the achiral nematic toroid ($\omega_{eq} = 0$) corresponds to the minimum of F provided that $a_4 > 0$. In contrast, the mirror symmetry is broken spontaneously whenever $a_2 < 0$ (and $a_4 > 0$). The achiral–chiral critical transition at $a_2 = 0$ belongs to the universality class of the mean-field Ising model. Therefore, we can immediately infer that the value of the critical exponent β in $\omega_{eq} \sim (-a_2)^{\beta}$ is $\frac{1}{2}$. To obtain the dependence of the coefficients a_i on the elastic constants and ξ, we need to evaluate the integral in eq. (1.8). For the bend, twist and saddle-splay energies we find:

$$\begin{aligned}\frac{F_3}{K_3 R_1} = {} & \frac{2\pi^2}{\xi}\left(\xi - \sqrt{\xi^2-1}\right) \\ & + \pi^2 \frac{\xi - 9\xi^3 + 6\xi^5 + 6\xi^2\sqrt{\xi^2-1} - 6\xi^4\sqrt{\xi^2-1}}{(\xi^2-1)^{\frac{3}{2}}}\omega^2 + \mathcal{O}\left(\omega^4\right),\end{aligned} \tag{1.26}$$

$$\frac{F_2}{K_2 R_1} = 4\pi^2 \frac{\xi^3}{(\xi^2-1)^{\frac{3}{2}}}\omega^2 + \mathcal{O}\left(\omega^6\right), \tag{1.27}$$

$$\frac{F_{24}}{K_{24} R_1} = -4\pi^2 \frac{\xi^3}{(\xi^2-1)^{\frac{3}{2}}}\omega^2. \tag{1.28}$$

Though the bend and twist energies are Taylor expansions in ω, the saddle-splay energy is exact. The large ξ asymptotic behavior of the elastic energy reads:[♡]

$$\frac{F}{K_3 R_1} \approx \frac{\pi^2}{\xi^2} + 4\pi^2\left(k - \frac{5}{16\xi^2}\right)\omega^2 + \frac{\pi^2}{2}\omega^4 + \mathcal{O}\left(\omega^6\right), \tag{1.29}$$

[♠] Explicitly: $\{K_i\} = \{K_1, K_2, K_3, K_{24}\}$

[♡] The fourth-order term in the bend energy for general ξ, that reduces to $\frac{\pi^2}{2} K_3 R_2 \xi \omega^4$ in eq. (1.29), is not given in eq. (1.26), because it is too lengthy.

where $k \equiv \frac{K_2 - K_{24}}{K_3}$ is the elastic anisotropy in twist and saddle-splay. The achiral configuration contains only bend energy. For sufficiently thick toroids, bend distortions are exchanged with twist and the mirror symmetry is broken spontaneously, as expected; see fig. 1.4. Interestingly, if $K_{24} > 0$ the saddle-

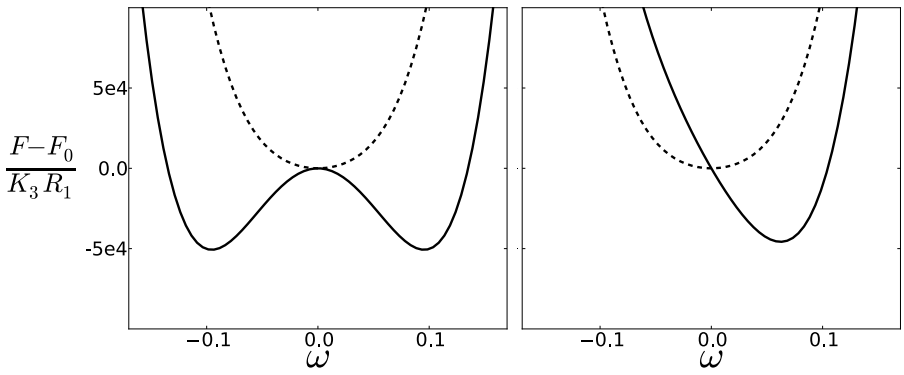

Figure 1.4: *Left panel:* The free energy as a function of ω for $\xi = 6$ (dashed) and $\xi = 5$ (solid), when $(K_2 - K_{24})/K_3 = 10^{-2}$. For $\xi = 5$ the chiral symmetry is broken spontaneously: the minimum values of the energy occur for nonzero ω. *Right panel:* The free energy as a function of ω for $q = 0$ (dashed) and $qR_2 = 10^{-3}$ (solid), when $\xi = 6$, $(K_2 - K_{24})/K_3 = 10^{-2}$ and $K_2/K_3 = 0.3$. For $qR_2 = 10^{-3}$ the chiral symmetry is broken explicitly: the minimum value of the energy occurs for a nonzero ω, because F contains a linear term in ω.

splay deformations screen the cost of twist. If $K_{24} < 0$ on the other hand, there is an extra penalty for twisting. Setting the coefficient of the ω^2 term equal to zero yields the phase boundary:

$$\begin{aligned} k_c &= \frac{-1 + 9\xi_c^2 - 6\xi_c^4 - 6\xi_c\sqrt{\xi_c^2 - 1} + 6\xi_c^3\sqrt{\xi_c^2 - 1}}{4\xi_c^2} \\ &\approx \frac{5}{16\xi_c^2} \qquad \text{if } \xi \gg 1. \end{aligned} \tag{1.30}$$

Figure 1.5 shows the phase diagram as a function of ξ and k. It is interesting to look at the critical behavior. The degree of twist close to the transition is

$$\alpha_{eq} \approx \omega_{eq} \approx 2\left(\frac{5}{16\xi^2} - k\right)^{1/2}, \tag{1.31}$$

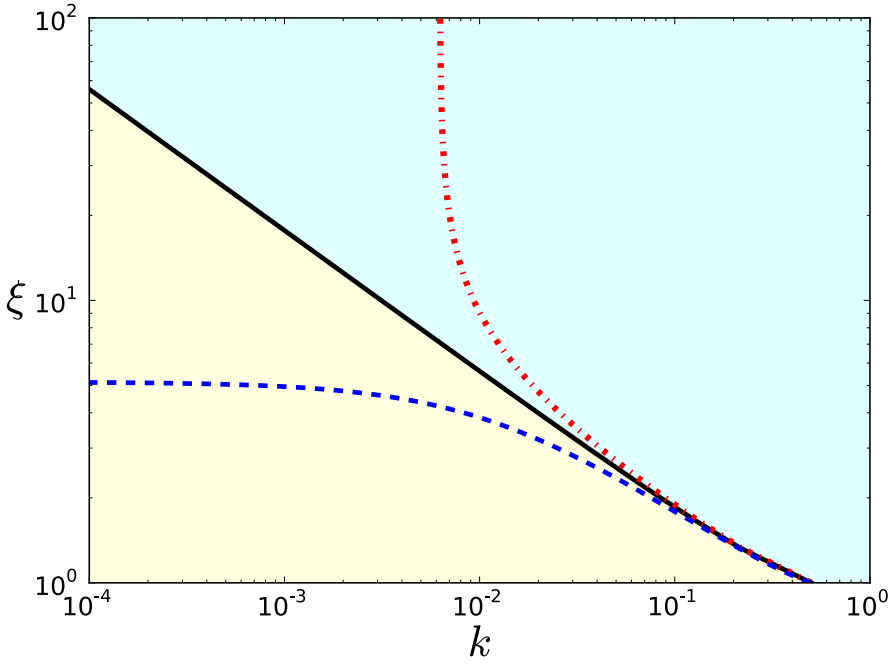

Figure 1.5: Phase diagram as a function of the toroidal slenderness and the elastic anisotropy in twist and saddle-splay constant, $k \equiv (K_2 - K_{24})/K_3$. The twisted (yellow region) and axial (cyan region) configuration are separated by a boundary line in the absence of an external field (solid black), when $\mathbf{H} = \sqrt{0.1K_3}/\left(\sqrt{\chi_a}R_2\right)\hat{\phi}$ (dashed blue) and when $\mathbf{H} = \sqrt{0.1K_3}/\left(\sqrt{\chi_a}R_2\right)\hat{\mathbf{z}}$ (dash-dotted red).

where we have used the identity $\sin\alpha_{eq} \approx \alpha_{eq}$ for small α_{eq}. Upon expanding $\xi = \xi_c + \delta\xi$ (with $\delta\xi < 0$) and $k = k_c + \delta k$ (with $\delta k < 0$) around their critical values ξ_c and k_c, respectively, we obtain the following scaling relations, while keeping k and ξ fixed, respectively:

$$\alpha_{eq} \approx \frac{\sqrt{5}}{2}\left(-\frac{\delta\xi}{\xi_c^3}\right)^{1/2}, \tag{1.32}$$

$$\alpha_{eq} \approx 2(-\delta k)^{1/2}. \tag{1.33}$$

Equations (1.32) and (1.33) are analogues to $m_{eq} \sim (-t)^{1/2}$, relating the equilibrium magnetization, m_{eq} (in the ferromagnetic phase of the Ising model in Landau theory), to the reduced temperature, t.

1.3.2 Effects of external fields and cholesteric pitch

Due to the inversion symmetry of nematics, $F[\mathbf{n}] = F[-\mathbf{n}]$, an external magnetic field, $\mathbf{H}$, couples quadratically to the components of $\mathbf{n}$ rather than linearly as in spin systems. The magnetic free energy contribution reads

$$F_m = -\frac{\chi_a}{2}\int \mathrm{d}V(\mathbf{n}\cdot\mathbf{H})^2, \tag{1.34}$$

where $\chi_a = \chi_\parallel - \chi_\perp$, the difference between the magnetic susceptibilities parallel and perpendicular to $\mathbf{n}$. Consequently, there is no explicit chiral symmetry breaking due to $\mathbf{H}$ as is the case in the Ising model. Rather, $\mathbf{H}$ shifts the location of the critical transition in the phase diagram. For concreteness, we will consider two different applied fields, namely a uniaxial field $\mathbf{H} = H_z\hat{\mathbf{z}} = H_z\sin(\psi)\hat{\mathbf{r}} + H_z\cos(\psi)\hat{\boldsymbol{\psi}}$ and an azimuthal field $\mathbf{H} = H_\phi\hat{\boldsymbol{\phi}}$, as if produced by a conducting wire going through the hole of the toroid. For $\mathbf{H} = H_z\hat{\mathbf{z}}$ we find:

$$\begin{aligned} F_m &= -\pi^2\chi_a H_z^2 R_1 R_2^2 \xi^2\left(2\xi\left(\xi - \sqrt{\xi^2-1}\right) - 1\right)\omega^2 \\ &\approx -\frac{\pi^2}{4}\chi_a H_z^2 R_1 R_2^2\omega^2 \qquad \text{if } \xi \gg 1. \end{aligned} \tag{1.35}$$

For a positive χ_a this energy contribution is negative, implying that a larger area in the phase diagram is occupied by the twisted configuration. The new phase boundary — fig. 1.5 — which is now a surface in the volume spanned by ξ, k and H_z instead of a line, reads

$$\begin{aligned} k_c &= \frac{1}{(4\xi_c^2)}\left[-1+9\xi_c^2-6\xi_c^4-6\xi_c\sqrt{\xi_c^2-1}+6\xi_c^3\sqrt{\xi_c^2-1}\right. \\ &\quad \left.-\frac{\chi_a(H_z)_c^2R_2^2}{K_3}\left(\xi_c^2-1\right)\xi_c\left(-2\xi_c+2\xi_c^3+\sqrt{\xi_c^2-1}-2\xi_c^2\sqrt{\xi_c^2-1}\right)\right] \\ &\approx \frac{5}{16\xi_c^2}+\frac{\chi_a(H_z)_c^2R_2^2}{16K_3} \quad \text{if } \xi \gg 1. \end{aligned} \tag{1.36}$$

In contrast, an azimuthal field favors the axial configuration, contributing a positive ω^2-term to the energy when $\chi_a > 0$:

$$\begin{aligned} F_m &= -\pi^2\chi_a H_\phi^2 R_1 R_2^2+\frac{2\pi^2}{3}\chi_a H_\phi^2 R_1 R_2^2\xi \\ &\quad\times\left(2\xi^2\left(\xi-\sqrt{\xi^2-1}\right)-\sqrt{\xi^2-1}\right)\omega^2 \\ &\approx -\pi^2\chi_a H_\phi^2 R_1 R_2^2+\frac{\pi^2}{2}\chi_a H_\phi^2 R_1 R_2^2\omega^2 \quad \text{if } \xi \gg 1. \end{aligned} \tag{1.37}$$

Consequently, this yields a shifted phase boundary, see fig. 1.5:

$$\begin{aligned} k_c &= \frac{1}{(4\xi_c^2)}\left[-1+9\xi_c^2-6\xi_c^4-6\xi_c\sqrt{\xi_c^2-1}+6\xi_c^3\sqrt{\xi_c^2-1}\right. \\ &\quad \left.-\frac{2\chi_a(H_\phi)_c^2R_2^2}{3K_3}\left(\xi_c^2-1\right)\left(1+\xi_c^2-2\xi_c^4+2\xi_c^3\sqrt{\xi_c^2-1}\right)\right] \\ &\approx \frac{5}{16\xi_c^2}-\frac{\chi_a(H_\phi)_c^2R_2^2}{8K_3} \qquad \text{if } \xi \gg 1. \end{aligned} \tag{1.38}$$

Similar results of eq. (1.35) to eq. (1.38) hold for an applied electric field $\mathbf{E}$ instead of a magnetic field; the analog of χ_a is the dielectric anisotropy. There could however be another physical mechanism at play in a nematic insulator, namely the flexoelectric effect [154, 169]. Splay and bend deformations induce a polarisation

$$\mathbf{P} = e_1\mathbf{n}\nabla\cdot\mathbf{n}+e_3\mathbf{n}\times\nabla\times\mathbf{n}, \tag{1.39}$$

where e_1 and e_3 are called the flexoelectric coefficients. Note that the first term in eq. (1.39) is irrelevant for the divergence-free ansatz. A coupling of $\mathbf{P}$ with $\mathbf{E}$:

$$F_P = -\int dV \mathbf{P} \cdot \mathbf{E} \tag{1.40}$$

could potentially lead to a shift of the transition. In the particular case when $\mathbf{E} = E_z\hat{\mathbf{z}} = E_z \sin(\psi)\hat{\mathbf{r}} + E_z \cos(\psi)\hat{\boldsymbol{\psi}}$, however, the ω^2 contribution from eq. (1.40) vanishes, thus not yielding such a shift.

If we now consider toroidal cholesterics rather than nematics, the chiral symmetry is broken explicitly, fig. 1.4. A cholesteric pitch of $2\pi/q$ gives a contribution to the free energy of:

$$F_{cn} = K_2\, q \int \mathrm{d}V \;\; \mathbf{n} \cdot \nabla \times \mathbf{n}. \tag{1.41}$$

Substituting eq. (1.23) yields:

$$\begin{aligned} F_{cn} &= -8\pi^2 K_2\, q\, R_1 R_2\, \xi \left(\xi - \sqrt{\xi^2 - 1}\right) \omega + \mathcal{O}\left(\omega^3\right) \\ &\approx -4\pi^2 K_2\, q\, R_1 R_2\, \omega + \mathcal{O}\left(\omega^3\right) \qquad \text{if } \xi \gg 1. \end{aligned} \tag{1.42}$$

Therefore, at the critical line in the phase diagram spanned by k and ξ, the degree of twist or surface angle scales (for large ξ) with the helicity of the cholesteric as:

$$\alpha_{eq} \approx \left(2K_2 R_2\, q/K_3\right)^{1/3} \sim q^{1/3}. \tag{1.43}$$

This is the analog scaling relation of $m_{eq} \sim H^{1/3}$ in the mean-field Ising model.

1.3.3 Results for the two-parameter ansatz

Motivated by experiments [55], we can introduce an extra variational parameter γ to allow for splay deformations, in addition to ω:

$$n_\psi = \omega \frac{\xi r/R_2}{\xi + \gamma \frac{r}{R_2} \cos\psi}. \tag{1.44}$$

(Note that eq. (1.23) is recovered by setting $\gamma = 1$ in eq. (1.44).) In section 1.3.1 analytical results for $\gamma = 1$ were presented. In this subsection we will slightly improve these results by finding the optimal value of γ numerically. First, we discretize the azimuthally symmetric director field in the r and ψ direction.

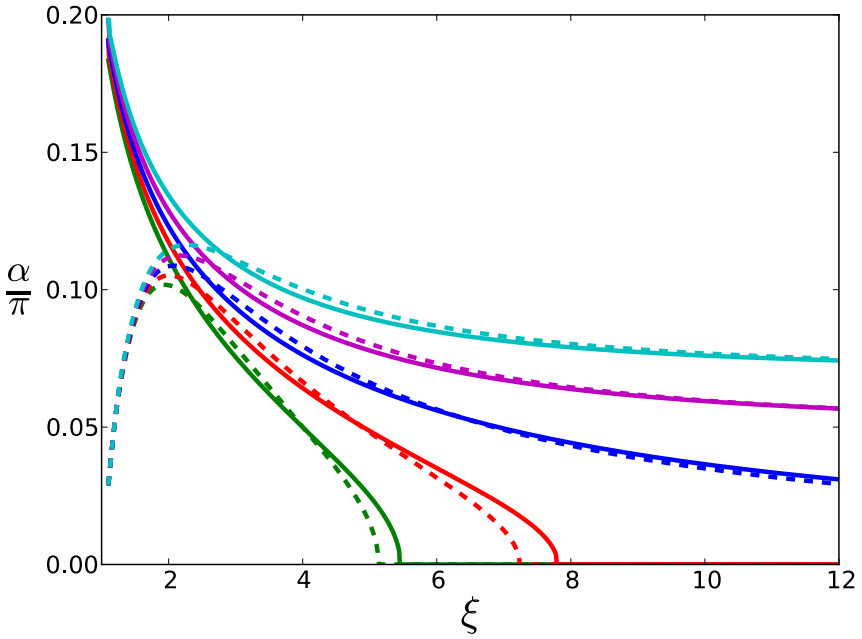

Figure 1.6: Twist angle α (in units of π) at $\psi = \pi/2$ versus the slenderness ξ for $k = 0.012$ (green), $k = 0.006$ (red), $k = 0$ (blue), $k = -0.006$ (magenta) and $k = -0.012$ (cyan). The dashed lines represent α for $\gamma = 1$, the solid lines represent α found for the optimal γ.

Next, we compute the Frank free energy density eq. (1.8) by taking finite differences [158] — see appendix section G.1 for details — of the discretized nematic field. After summation over the volume elements the Frank free energy will become a function of ω and γ for a given set of elastic constants and a given aspect ratio. Because of the normalisation condition on $\mathbf{n}$, the allowed values for ω and γ are constrained to the open diamond-like interval for which $-\xi < \gamma < \xi$ and $\frac{|\gamma|-\xi}{\xi} < \omega < \frac{\xi-|\gamma|}{\xi}$ holds.

The minima of the energy surface can be found by employing the conjugate gradient method — see appendix N for details. We have looked at the difference between the $\gamma = 1$ case and the case where the value of γ is chosen to minimise the energy. This was done for various choices of k. We have chosen the material properties of 5CB, i.e. $K_1 = 0.64K_3$ and $K_2 = 0.3K_3$ [119]. The value of K_{24} has not been so accurately determined, but previous measurements [55, 147, 151, 152, 153, 155] seem to suggest that $K_{24} \approx K_2$, corresponding to $k \approx 0$.

We are interested in how the phase boundary changes when the variational parameter γ is introduced. Therefore, the twist angle α, evaluated at the surface of the torus at $\psi = \frac{\pi}{2}$, versus the slenderness ξ is shown in fig. 1.6. For the particular choices of k there are two noticeable differences between the single-parameter ansatz and the two-parameter ansatz. Firstly, for small values of ξ, α is changed significantly. Secondly, for larger values of ξ we see that if there is a chiral–achiral phase transition, ξ_c is shifted by a small amount. In fig. 1.7 we further investigate how introducing γ influences the phase boundary, by plotting the phase boundary as a function of the toroidal slenderness ξ and elastic anisotropy k for both γ as a variational parameter (solid) and for $\gamma = 1$ (dashed). Observe that, for both the small ξ and small k regime, the difference is significant.

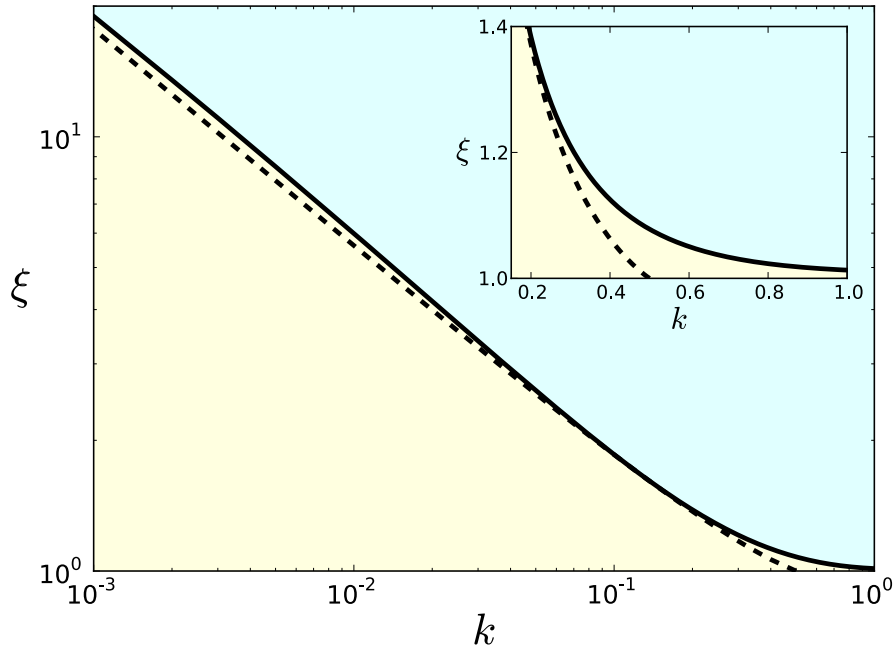

Figure 1.7: The phase boundary as a function of the toroidal slenderness ξ and elastic anisotropy k for γ as a variational parameter (solid) and for $\gamma = 1$ (dashed). The inset zooms in on the phase boundary for small ξ.

1.4 Experiments

Chiral symmetry breaking in toroidal nematics has been verified experimentally at Georgia Tech in the Fernandez-Nieves lab [55]. The experiment was done by first developing a method to construct nematic liquid crystals in a toroidal shape, and then exploiting the light-polarising properties of liquid crystals to measure the presence of a twist. Additionally, higher-order tori — tori with multiple handles — were measured as well.

The construction of the toroidal nematic droplet is done by injecting 5CB♠ through a rotating needle into a bath. The bath contains a mixture with a high yield stress. The mixture consists of 64.5 wt% ultra pure water, 30 wt% ethanol, 3 wt% glycerin, 1.5 wt% polyacrylamide microgels (carbopol ETD 2020), and 1 wt% polyvinyl alcohol. The polyvinyl alcohol ensures that the nematic liquid crystals align tangentially at the boundary as confirmed by making spherical droplets and checking their bipolar character. Also the continuous phase is neutralized to pH 7, where the sample transmission is more than 90% [125]. The most relevant property of this phase, however, is its yield stress, σ_y. During formation of the torus — the injection of 5CB into the bath — the stresses involved are larger than σ_y and hence the continuous phase essentially behaves as if it were a liquid. The combination of the viscous drag exerted by the outer phase over the extruded liquid crystal and its rotational motion causes the liquid crystal to form a curved jet, as shown in fig. 1.8 A, which eventually closes onto itself, resulting in a toroidal nematic droplet, such as that shown in fig. 1.8 B in bright field and in fig. 1.8 C between cross-polarizers. Once the torus has been formed, the elasticity of the continuous phase provides the required force to overcome the surface tension force that would naturally tend to transform the toroidal droplet into a spherical droplet [94]. Remarkably, when these droplets are observed along their side view under cross polarizers, their central region remains bright irrespective of the orientation of the droplet with respect to the incident polarization direction, as shown in fig. 1.8 D–F; the corresponding bright-field images are shown in fig. 1.8 G–I. Note that for an axial torus with its director field along the tube, the cross-polarized image should appear black for an orientation of 0 and 90° with respect to the incident polarization direction. Hence our result is suggestive of a twisted structure. In fact, twisted bipolar droplets also have a central bright region, when viewed between cross-polarizers, irrespective of their orientation [146, 157, 161, 163].

♠5CB is short for 4-n-pentyl-4'-cyanobiphenyl which is a commonly used material for liquid crystals.

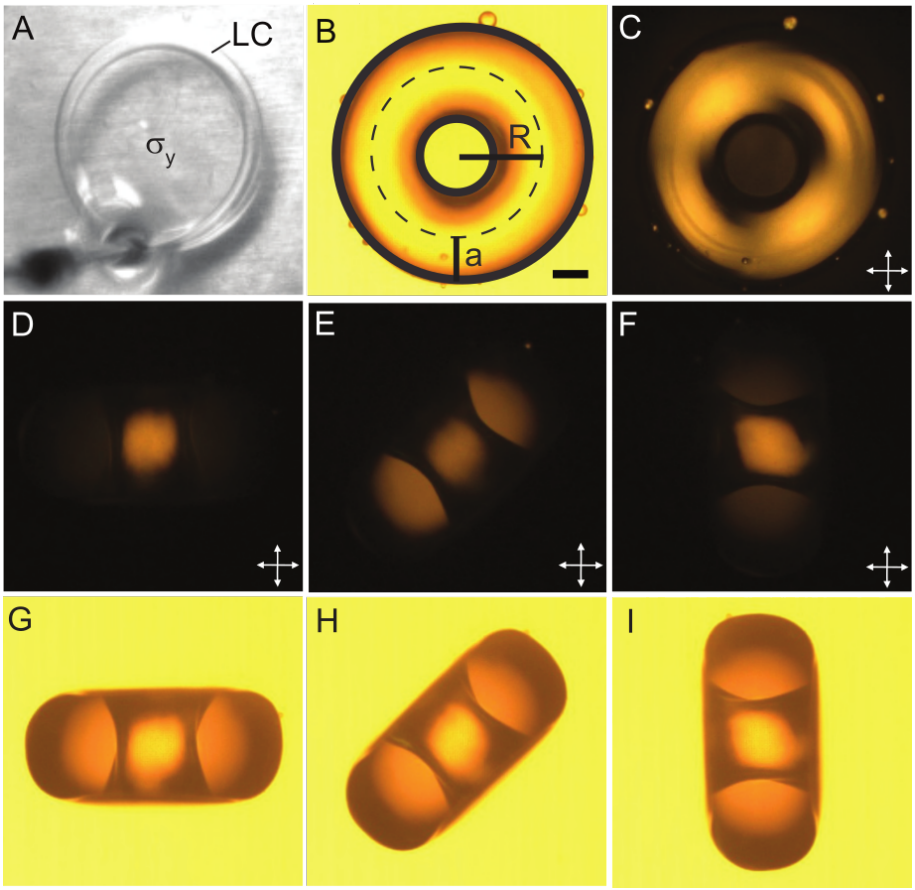

Figure 1.8: Toroidal droplets. (A) Formation of a toroidal liquid crystal droplet inside a material with yield stress σ_y. (B and C) The top view of a typical stable toroidal droplet of nematic liquid crystal, having tube and inner radii a and R, is shown in (B) when viewed in bright field and in (C) when viewed under cross-polarizers. (D–F) Side view of a typical toroidal droplet with $\xi = 1.8$ when viewed under cross-polarizers for orientations of 0°, 45°, and 90° with respect to the incident polarization direction. Note that the center part of the toroid remains bright irrespective of its orientation. (G–I) Corresponding bright-field images. The dark regions of the toroid in these images are due to light refraction. (Scale bar: 100μm.) [55]

The results are then quantified by measuring the twist angle in the toroidal droplets along the $\hat{z}$ direction, from $(r = a, \theta = 90^\circ)$ to $(r = a, \theta = 270^\circ)$, see fig. 1.2. The method relies on the fact that linearly polarized light follows the twist of a nematic liquid crystal if the polarization direction is either parallel or perpendicular to the nematic director at the entrance of the sample, provided the Mauguin limit is fulfilled [89]; the corresponding mode of propagation is referred to as extraordinary or ordinary waveguiding, respectively. We then image the torus is from above (fig. 1.9 A), rotate the polarizer to ensure that the incident polarization direction is parallel or perpendicular to the nematic director at $(r = a, \theta = 90^\circ)$, and then rotate the analyzer by an angle ϕ_{exit} with respect to the polarizer while monitoring the transmitted intensity, T. The minimum in T, shown in fig. 1.9 B, reflects the lack of light propagation through the analyzer, indicating that the incident polarization direction has rotated an amount τ such that it is perpendicular to the analyzer after exiting the torus at $(r = a, \theta = 270^\circ)$. The image of the torus in this situation exhibits four black regions where extinction occurs, as shown in fig. 1.9 C; these correspond to waveguiding of ordinary and extraordinary waves. It is along these regions that we measure T. The counterclockwise rotation of the incident polarization direction by an angle of -0.98 exactly corresponds to the twist angle of the nematic along the $\hat{z}$ direction through the center of the circular cross section. However, to increase the precision of our estimate, we fit the T vs. ϕ_{exit} results to the theoretically expected transmission [89], leaving τ as a free parameter. We find $\tau = (52.9 \pm 0.4)^\circ$ for $\xi = 3.5$. Moreover, within the experimentally accessed ξ-range, we find that the twist is nonzero and that it monotonously decreases with increasing aspect ratio, as shown in fig. 1.9 D. Remarkably, these features are captured by our theoretical calculations for large ξ, as shown by the dashed line in fig. 1.9 D. We note that the deviations of the experiment and the theory for small ξ result from the inadequacy of the ansatz in describing the highly twisted structures observed experimentally at these low values of ξ. This can be partially resolved by lifting the constraint that $\gamma = 1$. This introduces a second variational parameter in the ansatz, which allows the nematic field to splay. The result qualitatively captures the experimental trend for all aspect ratios, as shown by the solid line in fig. 1.9 D. By further comparing the experiment to the theory in the high ξ-region, we obtain a value for the saddle-splay elastic constant of $K_{24} = 1.02K_2$, which is slightly larger than the twist elastic constant, confirming our previous con-

clusions and supporting our interpretation on the relevance of saddle-splay distortions. However, our analysis cannot exclude the possibility of a slightly smaller value of K_{24} and hence of a twisted-to-axial transition for extremely large ξ.

1.5 Conclusions

We investigated spontaneous chiral symmetry breaking in toroidal nematic liquid crystals. As in the case of nematic tactoids [78, 116], the two ingredients for this macroscopic chirality are orientational order of achiral microscopic constituents and a curved confining boundary. This phenomenon occurs when both the aspect ratio of the toroid and $\frac{K_2-K_{24}}{K_3}$ are small. The critical behavior of this structural transition belongs to the same universality class as the ferromagnet–paramagnet phase transition in the Ising model in dimensions above the upper critical dimension. The analogues of the magnetization, reduced temperature and external field are the degree of twist (or surface angle), slenderness or $\frac{K_2-K_{24}}{K_3}$, and (cholesteric) helicity in liquid crystal toroids, respectively. Critical exponents are collected in table 1.1.

Liquid crystal toroid	Mean-field Ising model	Exponent
$\alpha_{eq} \sim (-\delta\xi)^{\beta}$	$m_{eq} \sim (-t)^{\beta}$	$\beta = 1/2$
$\alpha_{eq} \sim (-\delta k)^{\beta}$		
$\alpha_{eq} \sim q^{1/\delta}$	$m_{eq} \sim H^{1/\delta}$	$\delta = 3$

Table 1.1: Dictionary of the critical behavior of the structural transition in liquid crystal toroids and the thermal phase transition in the mean-field Ising model.

Thus, the helicity rather than an external field breaks the chiral symmetry explicitly. Remarkably, since an external field couples quadratically to the director field, it induces a shift of the phase boundary. An azimuthally aligned field favors the mirror symmetric director configuration, whereas a homogeneous field in the $\hat{z}$-direction favors the doubly twisted configuration.

A minimization of the elastic energy analogous to the one presented in this article for toroidal droplets has also been carried out for spherical droplets [161]. The analytical results qualitatively reproduce the twisted textures observed experimentally in spherical bipolar droplets [163]. In this case,

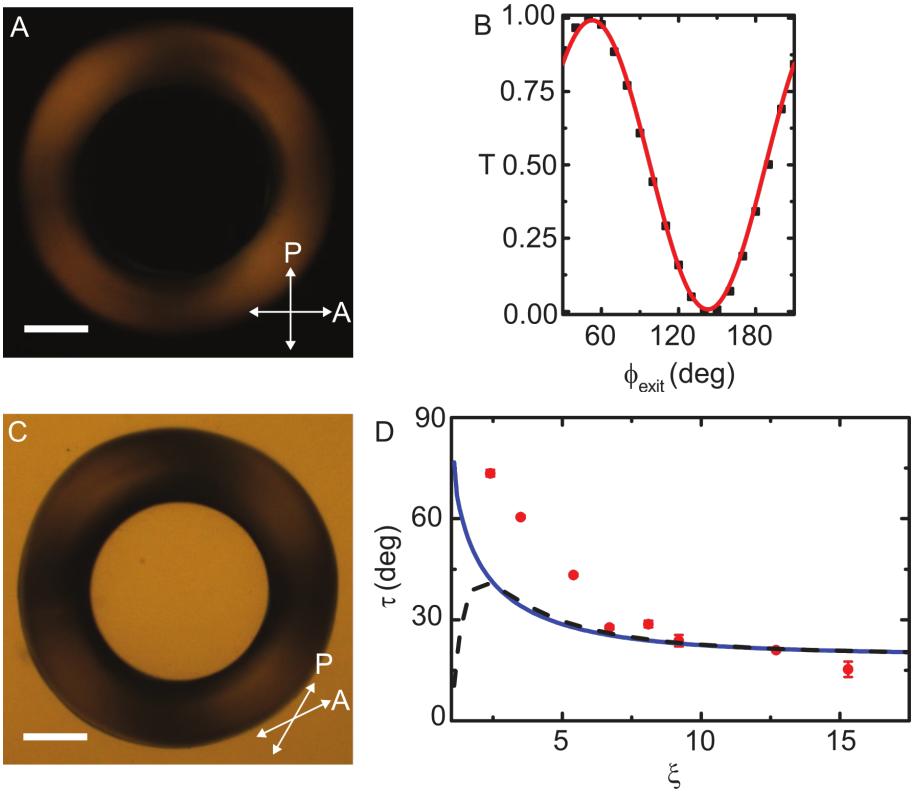

Figure 1.9: Determination of the twist angle and its dependence with slenderness. (A) A torus with $\xi = 3.5$ when viewed from the top and between cross-polarizers. (B) Transmission, T, as a function of the angle between the incident polarization direction and the analyzer, ϕ_{exit}. The line is a fit to the theoretical expectation in the Mauguin limit [89] with the twist angle, τ, as the only free parameter. We obtain $\tau = (52.9 \pm 0.4)^{\circ}$. (C) Top view of the same torus at the minimum of the transmission curve. We measure T along the four black regions that are observed, which are darkest for the indicated direction of the polarizer and analyzer. The sense of rotation of the analyzer indicates the nematic arrangement is right-handed; this likely results from the way the torus is generated, as all tori generated in the same way have the same handedness. (D) Twist angle as a function of ξ. The dashed line represents the theoretical prediction based on eq. (1.23), for $K_{24} = 1.02K_2$. The solid line represents the theoretical prediction based on the improved ansatz including the second variational parameter γ for the same value of K_{24}, where we have used the values $K_1 = 0.64K_3$ for 5CB [119]. (Scale bar: 200μm.) [55]

detailed measurements of the dependence of the twist angle on the elastic moduli were carried out by changing temperature which in turn affects the elastic moduli. The measured exponent β was 0.75 ± 0.1 for 8CB♠ and 0.76 ± 0.1 for 8OCB♡ [157], rather than the $\frac{1}{2}$ exponent we calculated in our mean field energy minimizations that entirely neglect thermal fluctuations.

♠8CB is short for 4'-n-octyl-4-cyano-biphenyl.
♡8OCB is short for 4-cyano-4'-octyloxybiphenyl.